AD-A063 744 JOHNS HOPKINS UNIV BALTIMORE MD DEPT OF EARTH AND PL--ETC F/G 8/3
AN EXPERIMENTAL STUDY OF THREE-LAYER CIRCULATION.(U)
JUL 78 M N RAFTENBERG N00014-75-C-0805
UNCLASSIFIED TR-14-SER-C NL

| OF |
ADA
063744

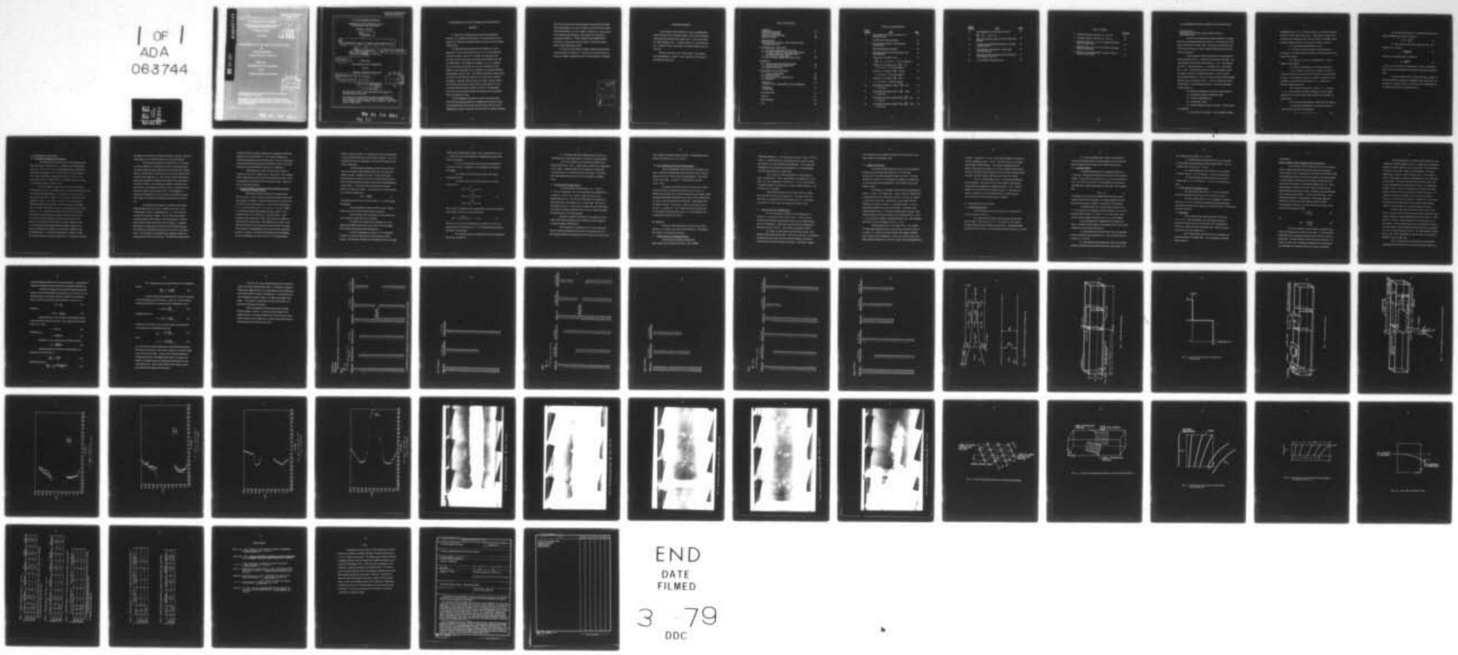

END
DATE
FILMED
3 -79
DDC

THE JOHNS HOPKINS UNIVERSITY

Departments of Earth & Planetary Sciences
and Mechanics & Materials Science

Baltimore, Maryland

July, 1978

AN EXPERIMENTAL STUDY OF THREE-LAYER CIRCULATION

By

Martin Neil Raftenberg

Technical Report No. 14 (Series C)

Sponsored by

THE OFFICE OF NAVAL RESEARCH

and the

NATIONAL SCIENCE FOUNDATION

Approved for public release.
Distribution unlimited.

THE JOHNS HOPKINS UNIVERSITY

Departments of Earth & Planetary Sciences
and Mechanics & Materials Science

Baltimore, Maryland

11 July, 1978

6 AN EXPERIMENTAL STUDY OF THREE-LAYER CIRCULATION.

By

10 Martin Neil Raftenberg

14 TR-14-SER-C

9 Technical Report No. 14 (Series C)

12 60 p.

Sponsored by

THE OFFICE OF NAVAL RESEARCH

and the

NATIONAL SCIENCE FOUNDATION

15 N00014-75-C-0805,
NSF-OCE76-18887

406 755

This research was supported by the Office of Naval Research, Fluid Dynamics Division, under Contract No. N00014-75-C-0805, and the National Science Foundation, under Grants No. OCE76-18887 and No. ATM76-22284.

AN EXPERIMENTAL STUDY OF THREE-LAYER CIRCULATION

ABSTRACT

A "three-layer circulation" flow, which occurs typically in estuaries, was modelled in the laboratory. The experiments were designed to test theoretical predictions made by Long in an earlier analysis of the problem.

The experiment consisted briefly of the following: a tank of length 496.6 cm and cross-section 37.2 cm x 15.9 cm was filled with two layers of water, each of 15.0 cm depth. The upper layer was fresh water and the lower layer was an NaCl-water solution with .25% or 1.00% salinity. After filling was completed, a 126.3 cm length at one end of the tank was blocked off, and the two fluid layers in this region were then thoroughly mixed, resulting in a homogeneous solution having salinity .125% or .50%. The partition separating the mixed region from the rest of the tank was removed, and a three-layer circulation flow ensued. Basically, fluid from the mixed region, having a density intermediate between the two layers outside of this region, was seen to flow out along the interface of these two layers. Simultaneously, flow in the reverse direction (into the mixed region) from the external layers was observed to occur.

Several techniques were used to visualize and study the flow. Potassium permanganate pellets were dropped into the tank from above. These produced dyed material lines upon dissolving, which were then photographed and used to determine velocity profiles at different locations.

The velocity profiles were then integrated to obtain estimates of fluxes. Moire fringe patterns were used to visualize interfaces between regions of differing salinities, as well as regions of turbulence. The use of this moire fringe pattern technique in experimental fluid mechanics is described in Appendix A. Finally, potassium permanganate dye in liquid form was added into the mixed region to visualize the cross-section of the outgoing slug of fluid.

All values for fluxes obtained in these experiments agreed with Long's predictions to within 24%. On the basis of the experimental results, the validity of assumptions made in Long's analysis is evaluated.

ACKNOWLEDGEMENTS

I wish to thank Professor Robert R. Long for suggesting this topic of research, for his financial support, and for many stimulating conversations pertaining to this research work. I also wish to thank Mr. Stuart Dickinson, Mr. J. Bradley Culkin, Ms. Kaye Burnett and Dr. L. Kantha for their many helpful comments during the course of this work.

Thanks are also due to Mr. Charles Mayes, who machined part of the apparatus. Finally, I wish to thank Mrs. Emily Evans, who typed this manuscript.

TABLE OF CONTENTS

TABLE OF ILLUSTRATIONS

LIST OF TABLES

AN EXPERIMENTAL STUDY OF THREE-LAYER CIRCULATION

I. INTRODUCTION

Description of the problem; Long's analysis; purpose of experimental work.

This work was motivated by a previous analysis of a general three-layer circulation problem by Long (1977). The situation has relevance to estuarine flow (Long, 1975). The problem as defined by Long will now be described, and Long's analysis and theoretical predictions will be summarized.

Long's analytical model (restricted to the two-dimensional case) is sketched in Fig. 1. Gravity acts in the minus z-direction. The lower boundary of the domain is described by $z = \zeta(x)$. The maximum value for ζ, occurring at some x, is set equal to zero. This defines the z = 0 line. This maximum locates the sill in the analytical model. The region of smaller x represents the estuary. The free surface occurs approximately at z = H for all x, but is allowed to deviate slightly from this value, as indicated in Fig. 1. In the y-direction the domain has thickness W_0 for all x except at the sill. There the y-thickness is a lesser value, W.

The following assumptions were made in Long's analysis:

(1) A hydrostatic pressure distribution exists;

(2) Velocity is independent of y;

(3) A steady-state exists;

(4) All three fluids are treated as inviscid. Viscous losses are neglected;

(5) The estuary is "overmixed". This condition is defined

mathematically in Eq. (3). A similar condition was imposed by Stommel and Farmer (1952, 1953) in their work. Long attaches a physical interpretation to this condition; namely, that the estuary is thoroughly mixed, so that any further increase in mixing will not further increase q_1.

(6) The Boussinesq approximation is used.

(7) The flow is laminar everywhere (except possibly in the estuary). No turbulent mixing takes place and no entrainment occurs outside of the estuary.

(8) Fluxes q_0, q_1 and q_2 are independent of x. This is implied by assumption 7.

(9) Velocity is independent of z within each fluid layer.

In order to obtain a "closed-form" solution, Long has restricted his attention to the special case in which no fresh-water influx occurs ($q_f = 0$) and layers S_0 and S_2 are of equal z-dimension ($h_1 = h_2$). In addition, the domain has a flat bottom ($\zeta \equiv 0$). At this point a further assumption was made.

(10) The flow is symmetric, so that $q_0 = q_2 = \frac{1}{2} q_1$ and $\eta_0 = \eta_2$. These constitute additional assumptions, since the upper boundary is a free surface (stress-free) and the lower boundary is a plate (no-slip).

Several theoretical predictions resulted from the analysis:

(1) The non-dimensionalized z-dimensions of the S_0, S_1 and S_2 layers at the sill are, respectively,

$$\eta_0 = \tfrac{1}{4}, \quad 1 - \eta_0 - \eta_2 = \tfrac{1}{2}, \quad \eta_2 = \tfrac{1}{4} \qquad (1)$$

(2) The non-dimensionalized z-dimension that the S_1 layer attains asymptotically at large x is given by

$$a = \tfrac{1}{2}\left[1-\left(1-\frac{W}{W_0}\right)^{\frac{1}{2}}\right] \tag{2}$$

(3) The volumetric flux in the outgoing S_1 layer, independent of x, is given by

$$q_1 = \frac{HW(H\Delta b_0)^{\frac{1}{2}}}{8} \tag{3}$$

where Δb_0, the buoyancy jump, is defined by

$$\Delta b_0 \equiv \frac{g(\rho_2-\rho_0)}{\rho_2} \tag{4}$$

ρ_0 and ρ_2 are the densities corresponding to S_0 and S_2, respectively. Thus a square-root-dependence is predicted between flux and buoyancy jump.

The experimental work to be described in the remainder of this report involved a laboratory investigation of this special case. Its purpose was to assess the degree of accuracy of these predictions and the degree of validity of the assumptions used.

II. EXPERIMENTAL PROCEDURE

2.1 Description of Apparatus and Procedure.

The experiments were performed in a tank with glass walls and a steel base, as shown in Fig. 2. The tank has inner dimensions 496.6 cm × 15.9 cm × 37.1 cm. Two plexiglass plates are taped to the inner walls at a distance of 126.3 cm from one end. These locate the sill. At the sill the flow is constricted with a gap of 2.78 cm. For convenience in future reference, define a coordinate system at the base of one plexiglass plate, as shown in Fig. 2.

The tank contained a single hole in its base for the purpose of filling and drainage. It was filled so that the initial salinity profile throughout its length was approximately a "step function", as shown in Fig. 3. This was accomplished as follows: A 15.0 cm layer of fresh water was added first. Then, a 15.0 cm layer of salt water was slowly added through the filling hole in the bottom of the tank from a second filling tank. Two values of salinity were used, corresponding to $\Delta b_0/g = .0025$ and $\Delta b_0/g = .01$. A glass plate was placed over the hole to minimize the jet effect, which would cause considerable mixing. There was a trade-off in selecting a filling-rate in that the faster the rate, the greater the mixing due to the jet effect previously mentioned as well as some mixing from the ensuing flow during filling. However, the slower the filling rate, the greater the mixing due to diffusion of salt into the upper layer. The optimum filling time was found to be about five hours for the two lower layer salinities used. A yellow dye, uranine, was added to the salt water to visualize the degree of mixing. The moire fringe pattern, to be described shortly, also served this purpose.

Once the tank was filled to the depth of 30.0 cm, the gap at the sill was blocked by a wooden plate clamped to the plexiglass plate. The estuary region was thus isolated from the rest of the tank. Kitchen blenders, inserted into the estuary region, were used to completely mix the fluid in this region (Fig. 4). After mixing, the fluid in the estuary region was homogeneous, having a density equal to the mean of those of the initial two layers. Once mixing was complete, the blenders were turned off and a few minutes were allowed to pass, enough time for the fluid in the estuary to nearly return to rest. Small quantities of potassium permanganate dye were used, first to show that the mixing in the estuary was complete and then that the fluid nearly returned to rest.

The experiment was begun by removing the wooden plate, thereby opening the gap at the sill. The digital timer (Fig. 4) was simultaneously turned on, establishing time $t = 0$. Later times were recorded from the timer's display. The mixed fluid in the estuary immediately began to flow outwards, towards increasing x, while the fluids in the two outside layers flowed into the estuary. A transient period followed, during which flow near the sill was highly unsteady. Next followed a period during which flow near the sill was very nearly steady. For the purpose of examining Long's analytical results, the steady period was the period of interest. This effectively steady period ended when either the estuary region became too highly stratified (the blenders were turned off before t = 0) or when the outgoing layer of fluid had approached the far wall of the tank. The time of commencement and duration of this steady period depended on $\Delta b_o/g$. They were determined by experimentation, using dyes for visualization.

Photographs of the region near the sill were taken at successive times, using a shutter time of 1/30 second. Three methods of flow visualization were used; dye pellets dropped from above, moire fringe patterns and liquid dye added to the estuary region. These will now be individually described.

2.2 Use of Dye Pellets for Experimental Determination of Velocity Profiles and Volumetric Fluxes.

Potassium permanganate pellets were dropped into the flow from above. In order to precisely control the position from which these pellets were dropped, a plank containing two holes was fitted over a portion of the top of the tank (Fig. 4). These holes were located at y = 7.9 cm (the center) and at x = 22.0 cm and x = 37.0 cm. Pellets were dropped simultaneously through both holes at about t = 60.0 seconds for Runs 6 and 7 with $\Delta b_o/g = .01$ and at about t = 240.0 seconds for Run 8 with $\Delta b_o/g = .0025$. These times were found to be in the effectively steady period. After hitting the free surface, these pellets sank and left a trace of purple dye in the form of a fine streak. These streaks were photographed at two successive times, separated by about 2.0 seconds. The digital clock appeared in the photographs, so the corresponding times were recorded. Two such photographs appear in Fig. 12 and Fig. 13. (Note that the timer does not appear in these prints; the times were read from the negatives.) Fig. 12 is from Run 6 and Fig. 13 is from Run 8, for which $\Delta b_o/g$ equals .01 and .0025, respectively.

An experimental determination of the velocity profile at these two x-locations could be obtained from these dye streaks by a simple procedure. Suppose that at time t_1 the streak from the pellet dropped at x (either 22.0 or 37.0 cm) had the measured location of x_1 (after taking into account the scale factor of the photograph) at some depth z. At the later time t_2 the streak had measured location x_2 at that same depth z. The approximate velocity at positive (x, z) was then computed from

$$u(x, z) = \frac{x_2 - x_1}{t_2 - t_1} \tag{5}$$

By repeating this procedure at discrete values of z, a velocity profile was obtained.

Several assumptions, which constitute sources of experimental error, were made in performing this calculation:

(1) The velocity vector was assumed to have only one non-zero component, namely that in the x-direction.

(2) Velocity was assumed to be independent of y. This neglects the boundary layers on the side walls as well as the highly three-dimensional region directly behind the sill.

(3) The two photographs were taken at a time separation of about 2.0 seconds, during which the streak displaced a finite distance. This procedure resulted in the computation of some "average"

velocity value at the particular depth z in the x-range between x_1 and x_2. There was some error introduced in identifying this result as the velocity at location x.

(4) The dyed streak had some slight motion independent of the fluid's motion. In particular, the dye appeared to continue to fall slightly.

(5) The flow was assumed to be steady, with velocity independent of time.

Volumetric fluxes are defined in terms of the velocity field u(x, z) by

$$q_0(x) = W_0 \int_{z_2(x)}^{H} u(x, z)\,dz$$

$$q_1(x) = W_0 \int_{z_1(x)}^{z_2(x)} u(x, z)\,dz \qquad (6)$$

$$q_2(x) = W_0 \int_{0}^{z_1(x)} u(x, z)\,dz$$

Since velocity was obtained from the photographs at discrete z_i locations, these integral expressions are approximated by

$$q_j(x) = W_0 \Delta z \sum_{i=1}^{n_j(x)} u(x, z_i) \;\; ; \quad j = 0, 1, 2 \qquad (7)$$

where $n_j(x)$ is the number of data points at x (either 22.0 or 37.0 cm) lying in the layer having salinity S_j. Δz is the spacing between adjacent data points, assumed equal.

Two additional sources of experimental error were introduced in these flux calculations:

(1) The replacement of the integral expressions in (6) by summations over discrete data points in (7) involved an approximation.

(2) The dye streaks were not always discernible at all z values at both times t_1 and t_2. In these cases velocity was not determined at all z values. Volumetric fluxes were computed by summing only over those values of z at which velocity was determined. Hence, the flux values obtained in these cases were low estimates (in absolute value).

2.3 Use of the Moire Fringe Pattern.

The front and back walls of the tank, at $y = -1.0$ and $y = 16.9$ cm, respectively, were covered by diffraction gratings in the x-range of -18 cm to 56 cm, and the z-range of 2.9 to 31.8 cm, approximately (Fig. 5). The tank was illuminated from behind by two fluorescent lamps, constituting a source of white light. This was the only light source used. A mylar sheet was hung on the back wall between the diffraction grating and the light source in order to disperse the light and eliminate glare from the photographs.

Appendix A contains a discussion of the production of moire fringes with diffraction gratings and the usefulness of these fringes in the study of salinity-stratified flows.

In this experiment fringe patterns were used to assess the degree of unwanted mixing during the process of filling the tank, to locate interfaces between homogeneous layers of salinity S_0, S_1 and S_2 and to locate regions of turbulent mixing in the flow. Fringe patterns can be observed in Figures 10, 11, 12, 13 and 14.

2.4 Use of Liquid Dye Added to the Estuary Region.

After the photographs of dye streaks from the pellets were taken, a potassium permanganate solution was poured into the estuary region near the sill. This was done at approximately $t = 100$ seconds for runs with $\Delta b_o/g = .01$ and at $t = 300$ seconds for runs with $\Delta b_o/g = .0025$.

The pattern of dye that formed in the estuary gave an indication of the degree of stratification that had occurred since $t = 0$. Shortly after pouring the dye, the fluid leaving the estuary appeared dyed. Subsequent photographs indicated the cross-section of the outgoing layer as well as certain internal features of this layer. Photographs of the dyed layer for $\Delta b_o/g = .01$ and $\Delta b_o/g = .0025$ are presented in Fig. 10 and Fig. 11, respectively. Fig. 14 shows the situation shortly after the dye began to emerge from the estuary. Note its usefulness in revealing internal feautres of the layer.

III. RESULTS.

Three runs of the experiment were performed; two runs with $\Delta b_o/g = .01$ (Runs 6 and 7) and one run with $\Delta b_o/g = .0025$ (Run 8). The results are presented in this section.

3.1 Velocity Profiles and Volumetric Fluxes.

Velocity data are presented in Appendix B.

Experimental velocity profiles from Runs 6 and 7 obtained with pellets dropped at $x = 22.0$ cm are shown in Fig. 6 and at $x = 37.0$ cm in Fig. 7. Velocity could not be determined at those z-values at which dye streaks were not discernible in the photographs. This was the case throughout the cross-section of the outgoing layer, in which turbulence caused the dye streaks to be quickly mixed.

Fig. 8 and Fig. 9 show experimental velocity profiles for Run 8, in which $\Delta b_0/g = .0025$. These profiles were obtained at $x = 22.0$ and $x = 37.0$ cm, respectively. Note that at $x = 37.0$ cm, where little or no turbulence appears to be present, a complete velocity profile (i.e., for all values of z) was obtained.

Experimental estimates of the volumetric fluxes are calculated from this velocity data by using Eq. (7). Theoretical values for these fluxes are computed by direct evaluation of Eq. (3). The results are presented in Tables 1 and 2 and compared in Tables 3 and 4.

3.2 Cross-section of the Outgoing Layer.

The non-dimensional z-thickness of the outgoing layer is called $(1-\eta_0-\eta_2)$ at the sill and a at large x (Fig. 1). These were determined experimentally by measuring the layer's cross-sectional thickness in the photographs. Theoretical values for these two quantities are obtained from Eqs. (1) and (2). The results are presented in Table 5.

For values of x intermediate between these two limits, some qualitative observations can be made. From Fig. 10 and Fig. 11, note that for both buoyancy jumps tested, the cross-sectional thickness of the layer rapidly diminishes with increasing x near the sill. Next follows a range of x in which the layer's z-thickness increases with increasing x, eventually settling to an asymptotic value.

3.3 Regions of Turbulence.

In the Experimental Procedure section and in the Appendix, discussions are presented concerning the use of moire fringe patterns and dye in revealing turbulent regions in the flow. Note that in both Fig. 12 and Fig. 13, fringe patterns consisting of straight lines are present outside of the outgoing layer. This indicates laminar flow in these regions.

The patterns are markedly different within the outgoing layer, however. In Fig. 13, for which $\Delta b_0/g = .0025$, a pattern of straight lines is clearly visible in most of the layer's interior. Yet there are regions in which this is not the case. Specifically, near the upper and lower boundaries of the layer, between x = 0 and approximately x = 40 cm, a fringe pattern appears but is not clearly defined. Small scale cells, perhaps turbulent eddies, are present indicating turbulent mixing. Such cells also appear in the layer's interior between approximately x = 8 and x = 25 cm, perhaps indicating an internal hydraulic jump. This turbulence in the layer's interior disappears at about x = 25 cm.

Referring now to Fig. 12, for which $\Delta b_0/g = .01$, note that the fringe pattern within the layer is quite different from that of Fig. 13. As in Fig. 13, a small scale cellular fringe pattern appears along the layer's upper and lower boundaries. In this case, however, these cells appear along the boundaries for the entire length of the photographed layer, between x = 0 and about x = 45 cm. These cells also appear in the layer's interior, beginning at about x = 26 cm. For lower values of x, no fringe pattern appears inside the layer. The probable interpretation of this feature is that at these low values of x, the flow is highly turbulent inside the layer, with large salinity variations occurring locally during the period of time for which the shutter of the camera was open (1/30 second).

Fig. 14, corresponding to $\Delta b_o/g = .01$ shows dye beginning to leave the estuary. This figure reveals a large degree of vorticity and mixing within the outgoing layer, beginning at about x = 7 cm. The flow appears to be largely laminar for smaller values of x. The layer also appears to increase in cross-sectional thickness at about this point. Again, perhaps an internal hydraulic jump is indicated.

IV. DISCUSSION AND CONCLUSIONS.

4.1 Velocity Measurements.

Two observations concerning velocity can be made directly from the measured velocities:

(1) Appreciable discrepancies appear between the data from Run 6 and Run 7, both with $\Delta b_o/g = .01$. The sources of error listed in the Experimental Procedure section account for this. Agreement between the data from the two runs is very close only in the lower layer at x = 22.0 cm.

(2) Long's assumptions that velocity is independent of z within each homogeneous layer and that complete symmetry exists between the upper and lower layers are not borne out by the data.

4.2 Volumetric Fluxes.

A complete velocity profile was obtained from Run 8 at $x = 37.0$ cm. Flux values calculated from this data are then relatively reliable. From Table 2 these values for q_0, q_1 and q_2 respectively are -44.5, 118. and -49.8 cm^3/sec. It is disturbing to see the extent to which they fail to satisfy conservation of volume (26%), which requires that

$$q_0 + q_2 = q_1 \tag{8}$$

The sources of error cited in the Experimental Procedure section should account for this discrepancy. All experimentally determined flux values are therefore subject to a large degree of uncertainty.

On the other hand, the velocity profile from Run 8 at the $x = 22.0$ cm location is incomplete in all three fluid layers, as are the velocity profiles at both $x = 22.0$ and $x = 37.0$ cm from Runs 6 and 7. The flux values computed from these data are even more doubtful.

Several conclusions are suggested by the computed flux values. In light of the large degree of uncertainty in these values, these conclusions must be viewed with caution.

(1) Experimentally determined values for q_2 are generally greater in absolute value than those for q_0. The one exception occurs in Run 6 at $x = 37.0$ cm.

(2) Experimentally determined values for q_2 are generally greater in absolute value than those predicted by Long's theory. The

one exception occurs in Run 7 at $x = 22.0$ cm.

(3) Experimentally determined values for q_0 are generally less in absolute value than those predicted by Long's theory. The one exception occurs in Run 7 at $x = 37.0$ cm.

(4) Experimentally determined values for q_0 are greater in absolute value at $x = 37.0$ cm than at $x = 22.0$ cm in all three runs.

(5) Experimentally determined values for q_2 are less in absolute value at $x = 37.0$ cm than at $x = 22.0$ cm in two out of three runs.

4.3 Cross-section of the Outgoing Layer.

The experimental values for $(1-\eta_0-\eta_2)$ agree reasonably well with the theoretical prediction of 0.50, as shown in Table 5.

The experimental values for a, the asymptotic z-thickness, however, are seen to be much greater than the theoretical prediction. The proposed hydraulic jump, which acts to thicken the layer, would account for this discrepancy.

4.4 Summation.

Long's analysis makes useful predictions of fluxes and of $(1-\eta_0-\eta_2)$. Of his assumptions, those significantly invalid are symmetry between the upper and lower layers, the independence of velocity on z within each layer, and laminar flow. This last assumption accounts for the discrepancies in a.

Moire fringe patterns have proven to be an invaluable tool in studying salinity in stratified flows. Their quantitative use merits further attention.

APPENDIX A:

The Use of Moire Fringe Patterns in Flow Visualization.

The usefulness of moire fringe patterns in revealing density fields in salinity-stratified flows has been previously discussed by Van Oss (1964), Oster, Wasserman and Zwerling (1964) and Baker (1969). The technique has its basis in the fact that when two diffraction gratings are superimposed, one lying on top of the other and inclined at some angle to the lower grating, a fringe pattern appears (Fig. 15). These fringes appear because the eye tends to connect adjacent points at which diffraction grating lines overlap. No light is transmitted through the two gratings at these points. As derived by Oster, *et al.*, if the diffraction gratings have line separation s and the upper grating is inclined at an angle θ to the lower grating, then the resulting fringes will have separation d and will be inclined at an angle φ to the lines of the lower grating, where

$$d = \frac{s}{2 \sin \frac{\theta}{2}} \tag{9}$$

and

$$\sin \varphi = \frac{\sin \theta}{2 \sin \frac{\theta}{2}} \tag{10}$$

If the lower grating is locally distorted or rotated in some region, the fringe pattern is altered in that region. In solid mechanics applications the lower grating is generally glued to the flat surface of a planar body. The upper grating is held fixed above the specimen. As the body is loaded, the accompanying alterations in the fringe pattern yield information concerning the specimen's surface deformation.

Moire fringe patterns are useful in fluid mechanics as well. Consider the situation sketched in Fig. 16. Suppose that two diffraction gratings are taped to opposite walls of a glass tank. The front grating is inclined at some angle relative to the back grating. The tank is lighted from the back by a collimated light source. When the tank is empty, a fringe pattern consisting of straight lines is seen when viewed from the front. Now suppose the tank is filled with salt water, with salinity monotonically decreasing with increasing z, but roughly independent of x and y. Thus, horizontal planes are regions of constant salinity. Since the the index of refraction of light in salt water, n, is a function of salinity, these planes are also regions in which n is constant. n decreases with increasing z. Note that this is very nearly the situation in the experiments discussed in this report, although regions of constant salinity are not exactly planar near the sill.

Further suppose that light from the light source is collimated in such a way that the light incident upon the back wall of the tank consists of planar wavefronts parallel to the back wall (Fig. 17). Note that such a wavefront, upon emerging from the front surface, is no longer planar. All rays perpendicular to the wavefront have been bent. The effect of this is that the diffraction grating on the back wall appears to a viewer in front of the tank to distort. The fringe pattern is thereby altered. Note that if salinity does in fact vary with y, the wavefront responds to some average value.

Oster, Wasserman and Zwerling (1964) have presented a relationship between the index of refraction field inside the tank, n(z), and the resulting alterations in the moire fringe pattern. They indicated a method of deriving their result, which will be presented explicitly here.

Consider the segment of the wavefront of light traversing the small section of the tank bounded by the planes z and $z+\Delta z$ (Fig. 18). By definition of index of refraction, the speed of light in the salt water at depth z is related to n(z) and the speed of light in a vacuum, c, by

$$v(z) = \frac{c}{n(z)} \tag{11}$$

Similarly,

$$v(z+\Delta z) = \frac{c}{n(z+\Delta z)} \tag{12}$$

Suppose that after a time increment Δt following the entrance of this wavefront segment into the tank, it has completely traversed the tank at $z+\Delta z$. Then

$$A = v(z+\Delta z)\Delta t \tag{13}$$

Substituting (12),

$$\Delta t = \frac{An(z+\Delta z)}{c} \tag{14}$$

Meanwhile at z, the wavefront has travelled a distance

$$y(z) = \frac{An(z+\Delta z)}{n(z)} \tag{15}$$

Approximating the wavefront as still being planar, its slope after time increment Δt is

$$\left(\frac{dy}{dz}\right)_z \simeq \frac{A-y(z)}{\Delta z} \tag{16}$$

Substituting from (15)

$$\left(\frac{dy}{dz}\right)_z \simeq \frac{A}{\Delta z}\left[\frac{n(z)-n(z+\Delta z)}{n(z)}\right] \tag{17}$$

Now replacing $n(z+\Delta z)$ by a truncated Taylor series expansion about z,

$$\left(\frac{dy}{dz}\right)_z \simeq -A\left(\frac{1}{n}\frac{dn}{dz}\right)_z \tag{18}$$

Consider a light ray perpendicular to this wavefront, entering the tank through the back wall at some z_b (Fig. 19). The ray emerges through the front wall at z_f, having an angle of inclination β, where

$$\beta = \arctan\left[\left(\frac{dy}{dz}\right)_{z=z_f}\right] \tag{19}$$

Substituting from (18)

$$\beta = \arctan\left[-A\left(\frac{1}{n}\frac{dn}{dz}\right)_{z=z_f}\right] \tag{20}$$

Assuming β to be small, the ray's average angle of inclination while traversing the tank is approximately given by

$$\beta_{avg} \simeq -\frac{A}{2}\left(\frac{1}{n}\frac{dn}{dz}\right)_{z=z_f} \tag{21}$$

Hence

$$z_b - z_f \simeq -\frac{A^2}{2}\left(\frac{1}{b}\frac{dn}{dz}\right)_{z=z_f} \tag{22}$$

Eq. (22) relates the vertical displacement of the diffraction grating on the back wall at elevation z_b that would be apparent to an observer right at the front wall of the tank. Using Eq. (22) and having determined through calibration the relationship between index of refraction and salinity, the salinity field can be quantitatively determined from the fringe pattern data. This procedure would be quite tedious, and for this reason does not appear in the literature.

From Eq. (22), note a property that has proven especially useful in the work presented in this report. In homogeneous regions of fluid (in which $\frac{dn}{dz}$ equals zero), the fringe pattern will be unaffected by the fluid and therefore consists of straight lines. At the interfaces between homogeneous regions, however, a complex fringe pattern will appear. This property, as previously noted by Baker (1969), is of great use in locating such interfaces.

Moire fringe patterns are also quite useful in locating turbulent regions in the flow. In turbulent regions salinity varies rapidly with time. If the characteristic time of this variation is much smaller than the camera shutter time, no stable fringe pattern appears. This property was also utilized in this work.

APPENDIX B.

Velocity Data

Data are presented for Runs 6, 7, and 8, as described in the text.

Run 6

$\frac{\Delta b_0}{g} = .01$

$t_1 = 64.21$ sec., $t_2 = 66.78$ sec.

Depth y(cm)	x = 22.0 cm *Velocity u(cm/sec)	x = 37.0 cm *Velocity u(cm/sec)
.23		
.47		
.70		
.93	-.53	-.59
1.17	-.53	-.65
1.40	-.56	-.70
1.63	-.60	-.71
1.87	-.62	-.72
2.10	-.64	-.73
2.33	-.67	-.75
2.57	-.69	-.75
2.80	-.70	-.74
3.04	-.72	-.74
3.27	-.72	-.74
3.50	-.73	-.74
3.74	-.73	-.75
3.97	-.73	-.75
4.20	-.73	-.75
4.44	-.73	-.75
4.67	-.72	-.75
4.90	-.73	-.75
5.14	-.74	-.75
5.37	-.75	-.75
5.60	-.75	-.75
5.84	-.75	-.75
6.07	-.75	-.75
6.30	-.75	-.74
6.54	-.75	-.73
6.77	-.75	-.72

Depth y(cm)	x = 22.0 cm Velocity u(cm/sec)	x = 37.0 cm Velocity u(cm/sec)
7.00	-.75	-.71
7.24	-.76	-.71
7.47	-.76	-.70
7.70	-.77	-.68
7.94	-.77	-.66
8.17	-.77	-.65
8.40	-.76	-.62
8.64	-.75	-.58
8.87	-.75	
9.11	-.75	
9.34	-.75	
9.57	-.75	
No measurement 9.81 through 19.14		
19.38	-.88	
19.61	-.85	
19.83	-.83	-.67
20.08	-.79	-.70
20.31	-.77	-.72
20.54	-.75	-.71
20.78	-.74	-.71
21.01	-.74	-.69
21.25	-.73	-.69
21.48	-.72	-.67
21.71	-.70	-.66
21.95	-.68	-.65
22.18	-.67	-.65
22.41	-.68	-.66
22.65	-.65	-.66

*A slot having no entry signifies that no measurement was able to be made at this depth.

Run 6 (continued)

Depth y(cm)	x = 22.0 cm *Velocity u(cm/sec)	x = 37.0 cm *Velocity u(cm/sec)
22.88	-.65	-.66
23.11	-.65	-.66
23.35	-.65	-.65
23.58	-.66	-.65
23.81	-.65	-.65
24.05	-.64	-.64
24.28	-.63	-.64
24.51	-.63	-.65
24.75	-.62	-.68
24.98	-.60	-.75
25.21	-.60	-.66
25.45	-.58	-.57
25.68	-.57	-.54
25.91	-.56	-.52
26.15	-.55	-.51
26.38	-.55	-.55
26.61	-.53	-.56
26.85	-.52	-.56
27.08	-.54	-.58
27.32		-.57
27.55		-.57
27.78		-.57
28.02		-.57
28.25		-.55
28.48		-.53
28.72		-.53
28.95		-.52
29.18		-.48
29.42		-.45
29.65		-.45
29.88		-.39

Run 7

$\frac{\Delta b_o}{g} = .01$

$t_1 = 68.01$ sec., $t_2 = 66.78$ cm

Depth y(cm)	x = 22.0 cm Velocity u(cm/sec)	x = 37.0 cm Velocity u(cm/sec)	Depth y(cm)	x = 22.0 cm Velocity u(cm/sec)	x = 37.0 cm Velocity u(cm/sec)
.23			7.08	-7.7	-7.8
.46			7.31	-7.8	-7.6
.69			7.54	-7.8	-7.3
.91		-6.1	7.77	-7.8	-7.1
1.14		-6.6	8.00	-7.8	-7.2
1.37		-7.0	8.23	-7.8	-7.1
1.60		-7.0	8.45	-7.8	-6.6
1.83		-7.2	8.68	-7.8	-6.6
2.06		-7.3	8.91	-7.8	
2.28		-7.3	9.14	-7.7	
2.51	-6.8	-7.5	9.37	-7.3	
2.74	-6.7	-7.8	No measurements		
2.97	-7.1	-7.9	9.60 through 19.19		
3.20	-7.2	-8.1	19.42	-7.8	
3.43	-7.2	-8.2	19.65	-7.6	
3.66	-7.2	-8.3	19.88	-7.5	-10.2
3.88	-7.2	-8.2	20.11	-7.2	- 9.8
4.11	-7.2	-8.1	20.34	-7.2	- 9.3
4.34	-7.2	-8.1	20.56	-6.7	- 8.9
4.53	-7.3	-8.1	20.79	-6.7	- 8.7
4.80	-7.3	-8.2	21.02	-6.6	- 8.3
5.03	-7.5	-8.2	21.25	-6.5	- 8.2
5.26	-7.5	-8.1	21.48	-6.3	- 7.9
5.48	-7.5	-8.1	21.77	-6.1	- 7.7
5.71	-7.6	-8.1	21.93	-5.8	- 7.7
5.94	-7.6	-8.2	22.16	-6.0	- 7.6
6.17	-7.6	-8.2	22.37	-5.8	- 7.3
6.40	-7.5	-8.2	22.62	-5.7	- 7.3
6.63	-7.6	-8.1	22.85	-5.6	- 7.3
6.85	-7.6	-7.9	23.08	-5.6	- 7.3

Run 7 (continued)

Depth y(cm)	x = 22.0 cm Velocity u(cm/sec)	x = 37.0 cm Velocity u(cm/sec)
23.31	-5.7	-7.3
23.53	-5.6	-7.2
23.76	-5.6	-7.1
23.99	-5.6	-7.0
24.22	-5.6	-6.7
24.45	-5.5	-6.6
24.68	-5.3	-6.7
24.90	-5.2	-6.7
25.3	-5.1	-6.7
25.36	-5.0	-6.5
25.59	-5.0	-6.3
25.82	-4.7	-6.1
26.05	-4.7	-6.1
26.28	-4.7	-6.0
26.50	-4.6	-6.0
26.73	-4.6	-5.8
26.96	-4.7	
27.19	-5.0	
27.42	-5.0	
27.65	-4.6	
27.88	-4.6	
28.10		
-28.33		
-28.56		
-28.78		
-29.00		
-29.50		
-29.73		

Run 8

$\frac{\Delta b_o}{g} = .0025$

$t_1 = 253.80$ sec, $t_2 = 256.3$

Depth y(cm)	x = 22.0 cm Velocity u(cm/sec)	x = 37.0 cm Velocity u(cm/sec)	Depth y(cm)	x = 22.0 cm Velocity u(cm/sec)	x = 37.0 cm Velocity u(cm/sec)
.28		-.06	8.61	-.37	-.34
.56		-.09	8.89	-.36	-.32
.83		-.13	9.17	-.34	-.27
1.11		-.16	9.44	-.33	-.20
1.39		-.17	9.72	-.32	-.12
1.67	-.28	-.20	10.00	-.31	-.04
1.94	-.29	-.22	10.28	-.29	+.13
2.22	-.31	-.23	10.56	-.27	.23
2.50	-.32	-.27	10.83	-.28	.29
2.78	-.32	-.29	11.11		.31
3.06	-.33	-.31	11.39		.39
3.33	-.34	-.33	11.67		.61
3.61	-.36	-.37	11.94		.98
3.89	-.37	-.40	12.22		1.03
4.17	-.39	-.41	12.50		1.04
4.44	-.40	-.43	12.78		1.04
4.72	-.42	-.43	13.06		1.04
5.00	-.44	-.43	13.33		1.06
5.28	-.44	-.43	13.61		1.06
5.56	-.44	-.44	13.89		1.04
5.83	-.43	-.44	14.17		1.02
6.11	-.43	-.43	14.44		1.00
6.33	-.42	-.43	14.72		1.03
6.67	-.42	-.43	15.00		1.09
6.94	-.41	-.42	15.28		1.18
7.22	-.40	-.42	15.56		1.22
7.50	-.39	-.42	14.82		1.19
7.788	-.38	-.41	16.11		1.17
8.06	-.38	-.40	16.39		1.11
8.33	-.37	-.39	16.67		1.09

Run 8 (continued)

Depth y(cm)	x = 22.0 cm Velocity u(cm/sec)	x = 37.0 cm Velocity u(cm/sec)
16.94		1.04
17.22		1.01
17.50		.96
17.78		.90
18.06		.61
18.23		.43
18.61		.30
18.89	-.26	.13
19.17	-.29	+.02
19.44	-.31	-.11
19.72	-.36	-.17
20.00	-.40	-.24
20.28	-.43	-.28
20.56	-.44	-.32
20.83	-.46	-.36
21.11	-.47	-.37
21.39	-.46	-.38
21.67	-.46	-.38
21.94	-.46	-.38
22.22	-.46	-.39
22.50	-.43	-.40
22.78	-.41	-.41
23.06	-.33	-.41
23.37	-.27	-.41
23.61	-.18	-.42
23.89	-.13	-.41
24.17	-.11	-.41
24.44	-.12	-.39
24.72	-.12	-.37
25.00	-.12	-.32

Depth y(cm)	x = 22.0 cm Velocity u(cm/sec)	x = 37.0 cm Velocity u(cm/sec)
25.28	-.12	-.30
25.56	-.13	-.28
25.83	-.12	-.24
26.11	-.11	-.24
26.39	-.11	-.24
26.67	-.10	-.23
26.94	-.10	-.21
27.22	-.08	-.18
27.50	-.07	-.17
27.78	-.08	-.14
28.06	-.07	-.13
28.33	-.07	-.11
28.61	-.06	-.08
28.89	-.04	-.07
29.17	-.04	-.04
29.44	-.03	-.03
29.22	-.03	-.02
30.00		-.01

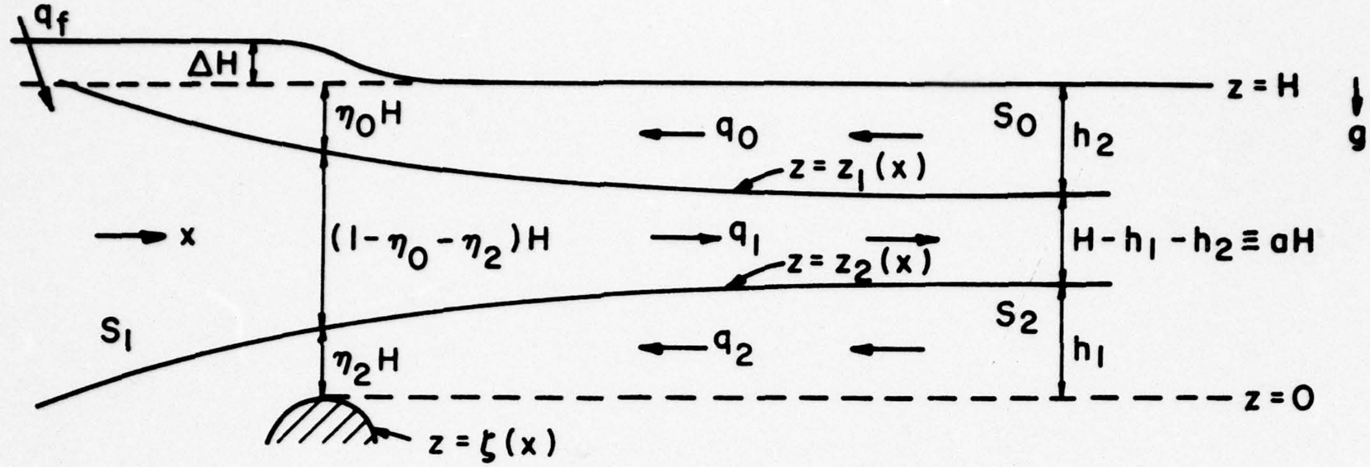

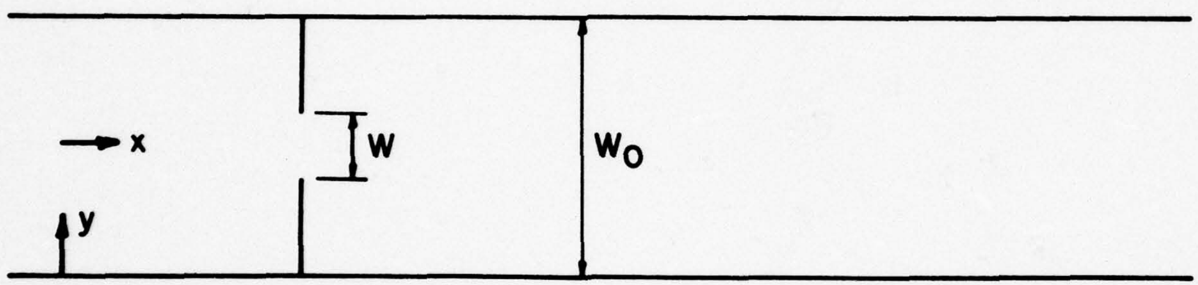

Fig. 1. Long's analytical model of an estuary; two orthogonal views

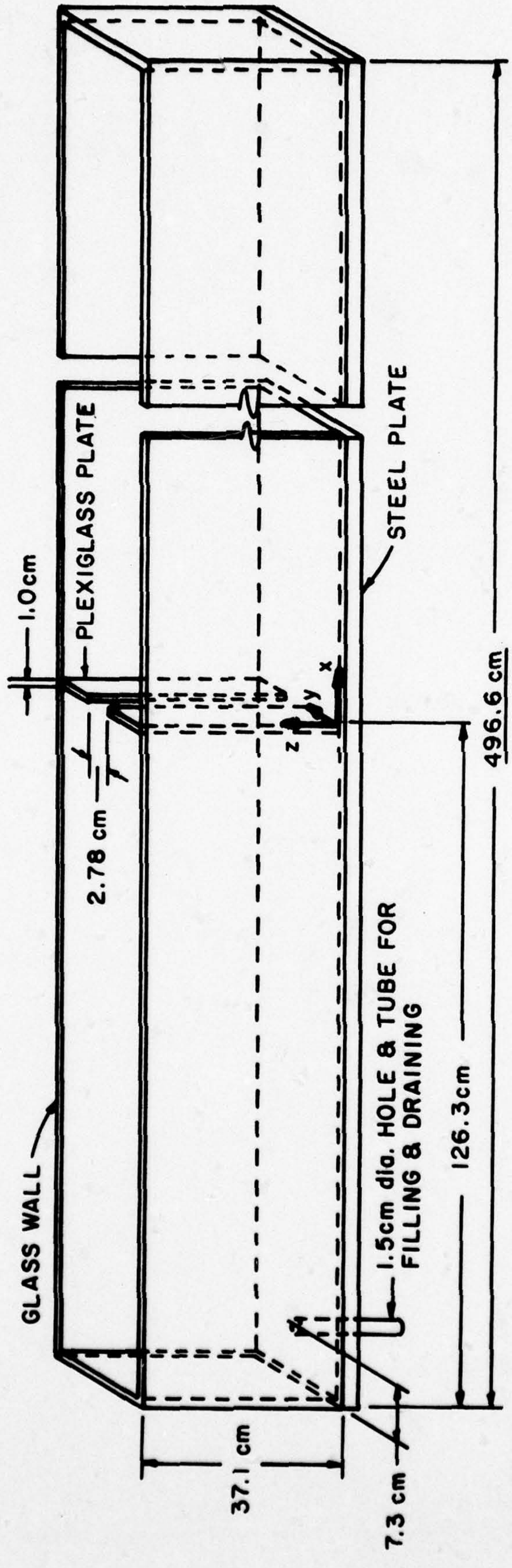

Fig. 2. The tank used in the experiment.

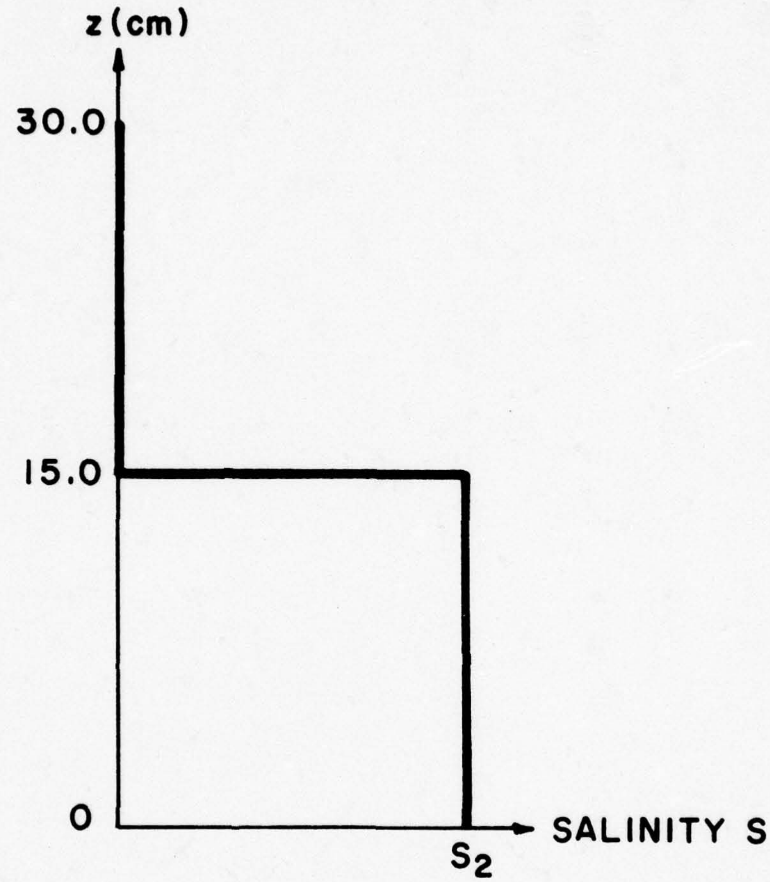

Fig. 3. Desired salinity profile at commencement of experiment.

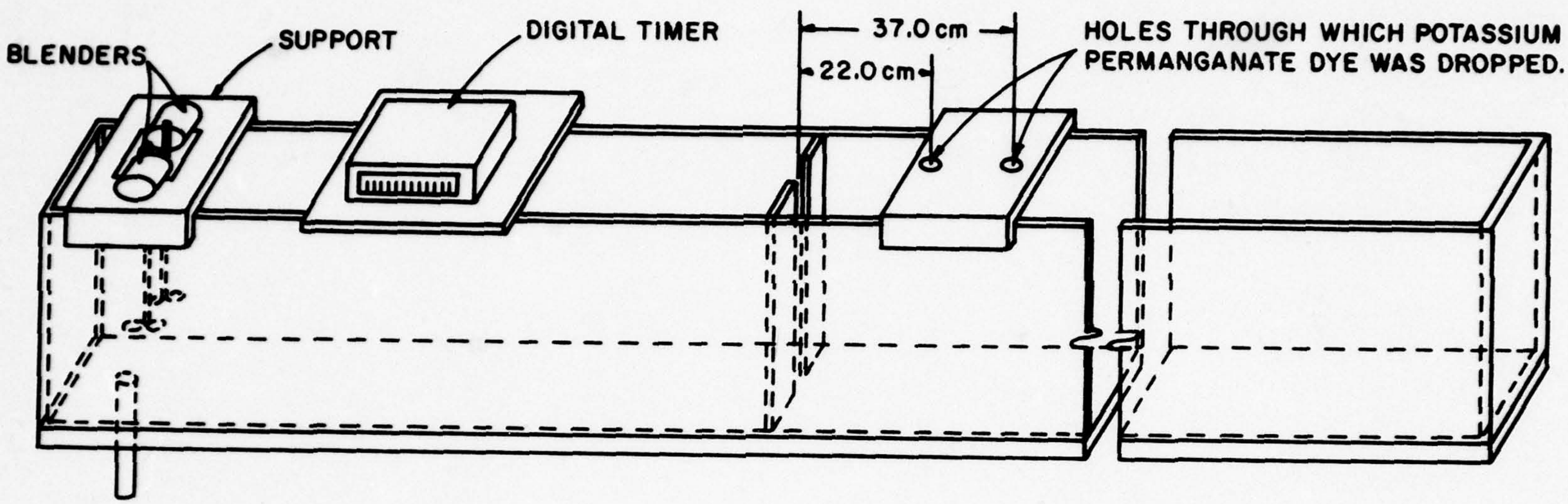

Fig. 4. Tank with peripheral equipment.

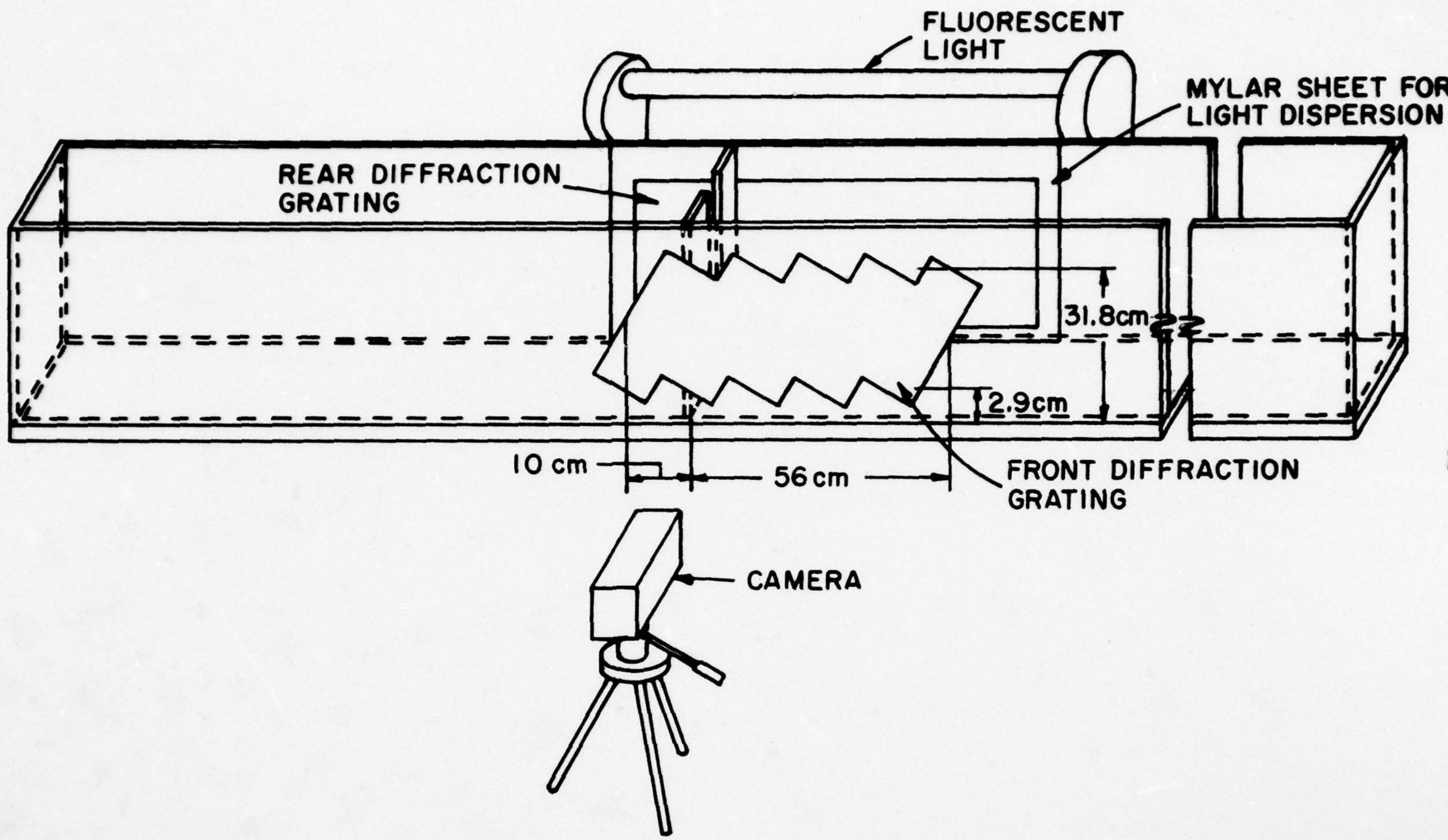

Fig. 5. Tank with equipment used in producing moire fringe patterns.

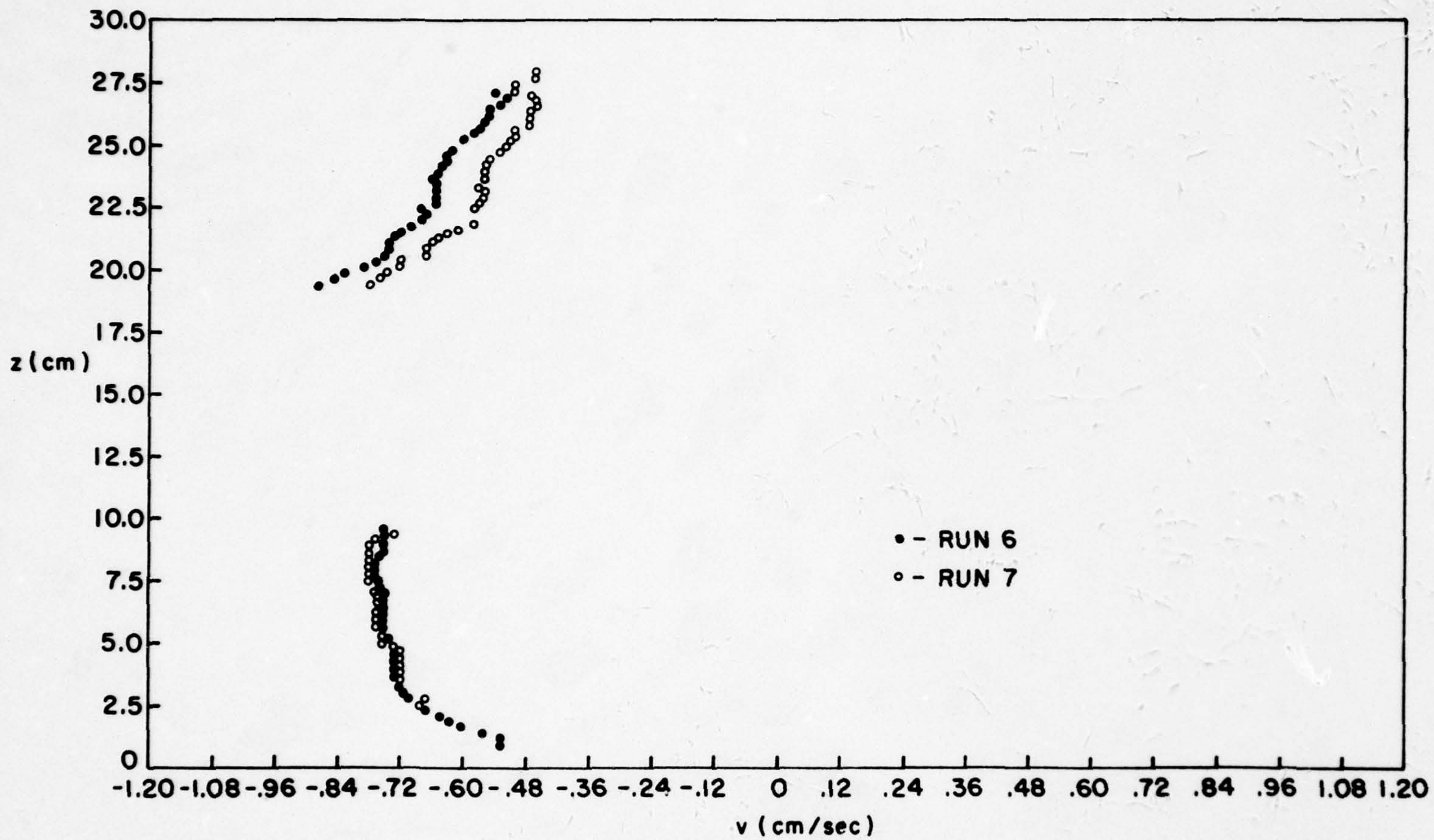

Fig. 6. Velocity vs. z for Runs 6 and 7;
$\frac{\Delta b_o}{g} = 0.1$, x = 22.0 cm, t = 60.0 sec (approx.)

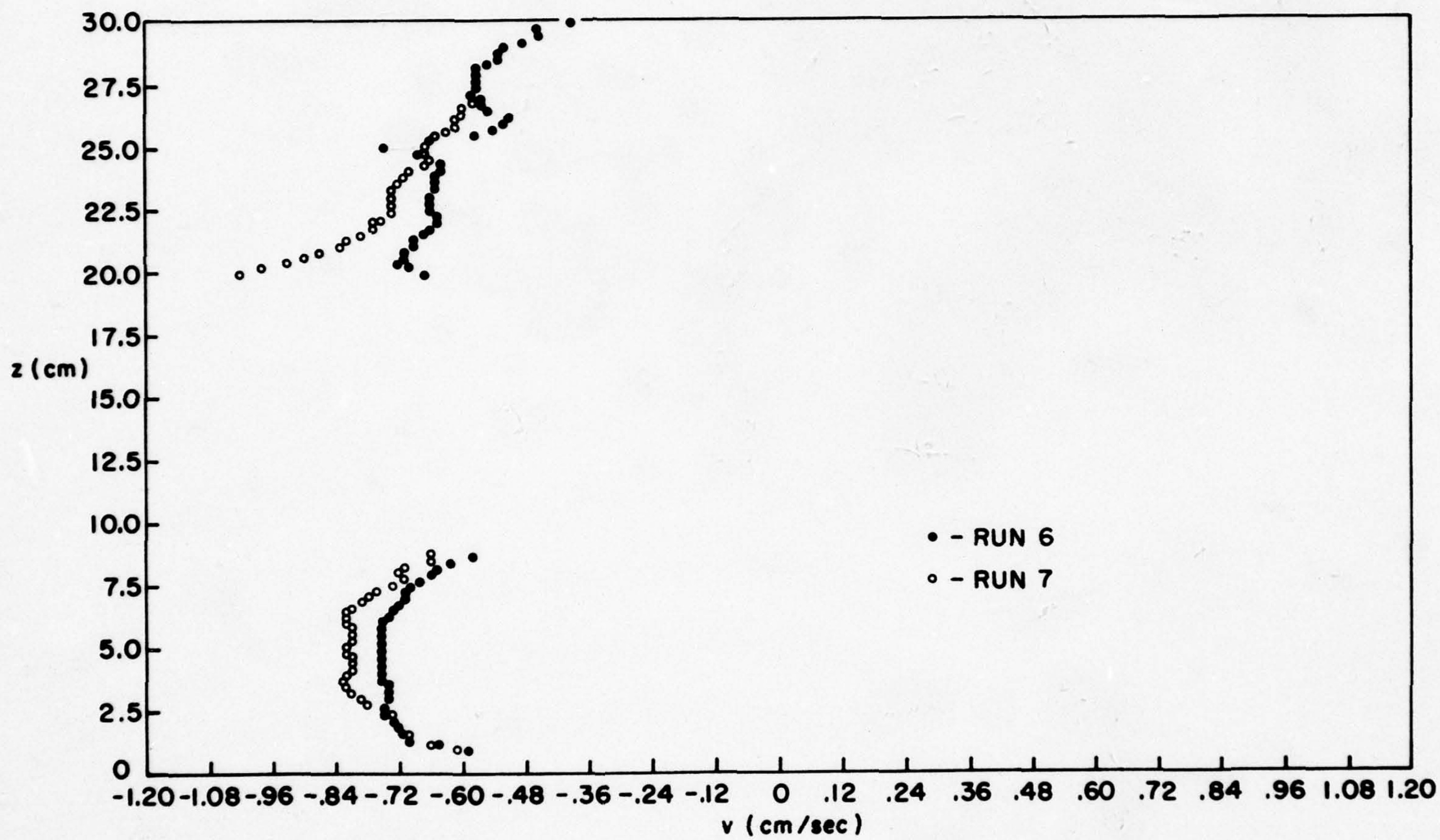

Fig. 7. Velocity vs. z for Runs t and y; $\frac{\Delta b_o}{g} = .01$,

x = 37.0 cm, t = 60.0 sec (approx.)

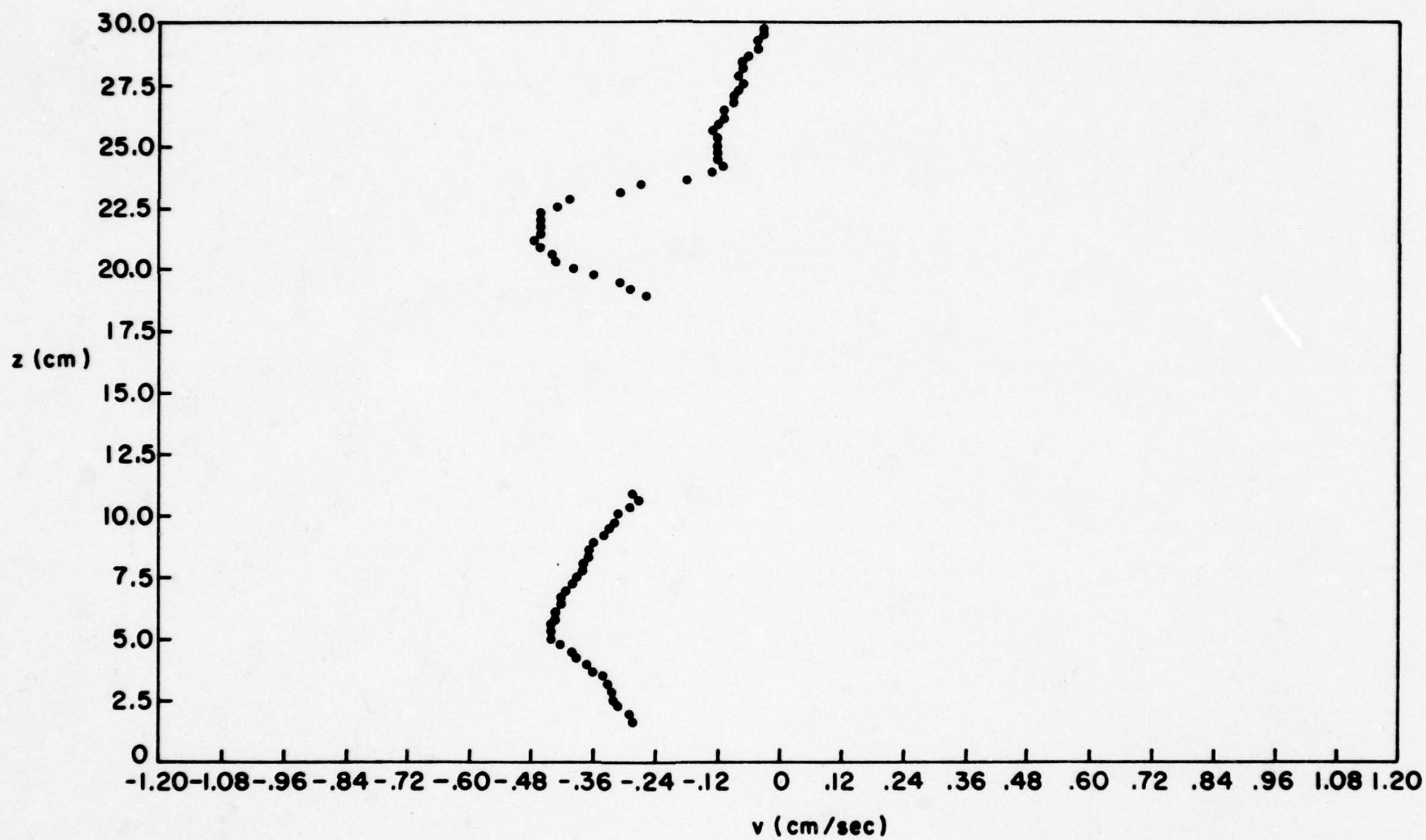

Fig. 8. Velocity vs. z for Run 8; $\frac{\Delta b_0}{g} = 0.0025$,

$x = 22.0$ cm, $t = 240.0$ sec (approx.)

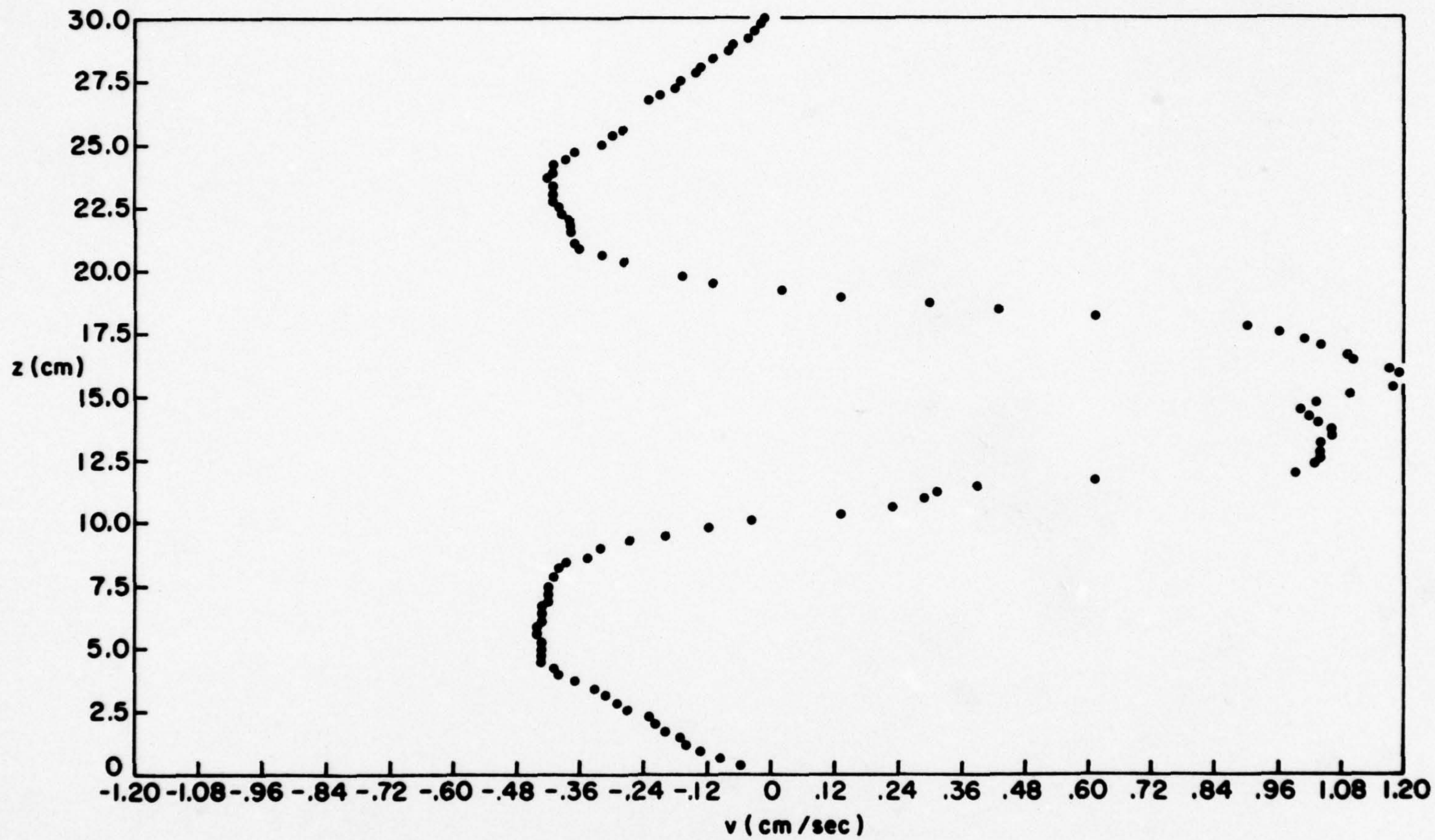

Fig. 9. Velocity vs. z for Run 8; $\frac{\Delta b_0}{g} = .0025$,

x = 37.0 cm, t = 240.0 sec (approx.)

Fig. 10. Dye leaving the estuary in Run 6; $\frac{\Delta b_o}{g} = 0.01$, $t = 223.0$ sec.

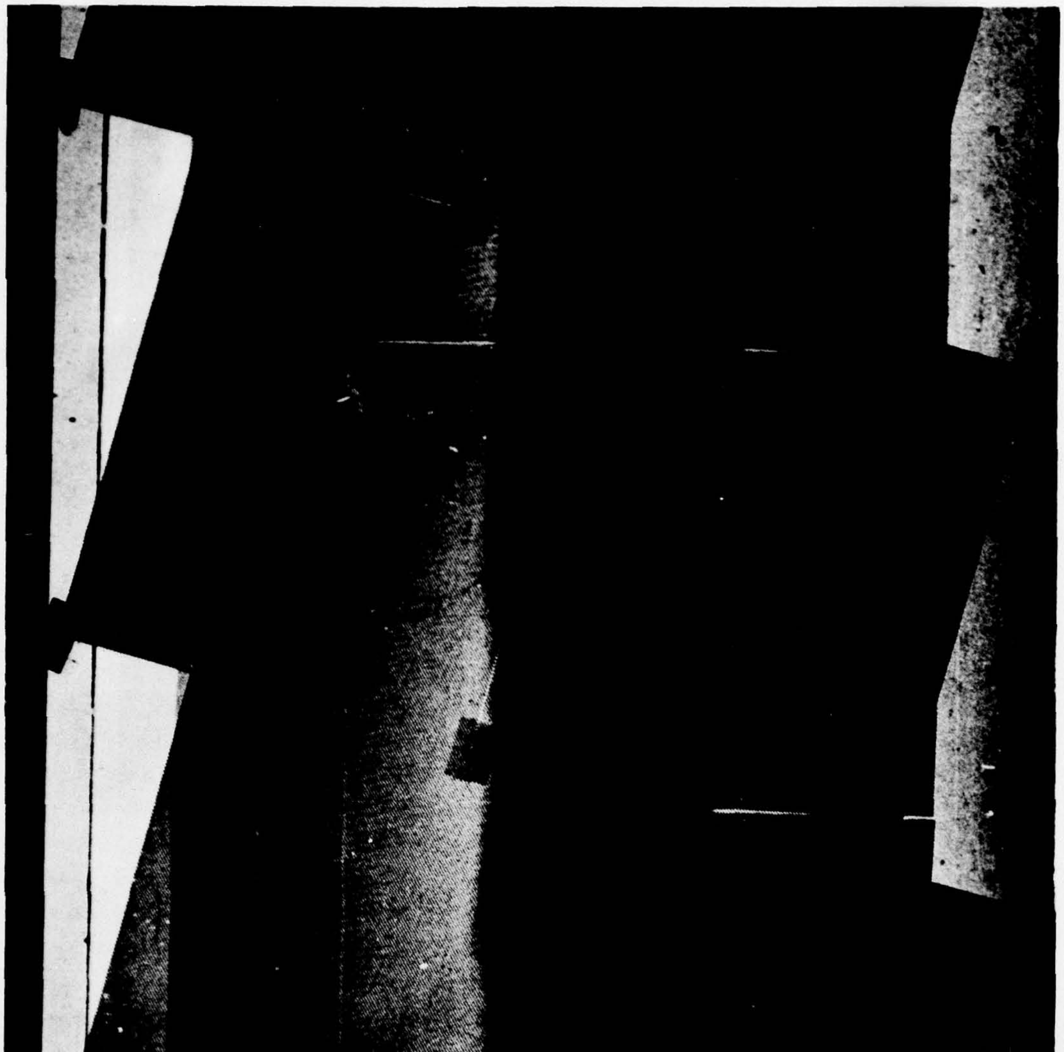

Fig. 11. Dye leaving the estuary in Run 8: $\frac{\Delta b_o}{g} = .0025$, $t = 389.7$ sec.

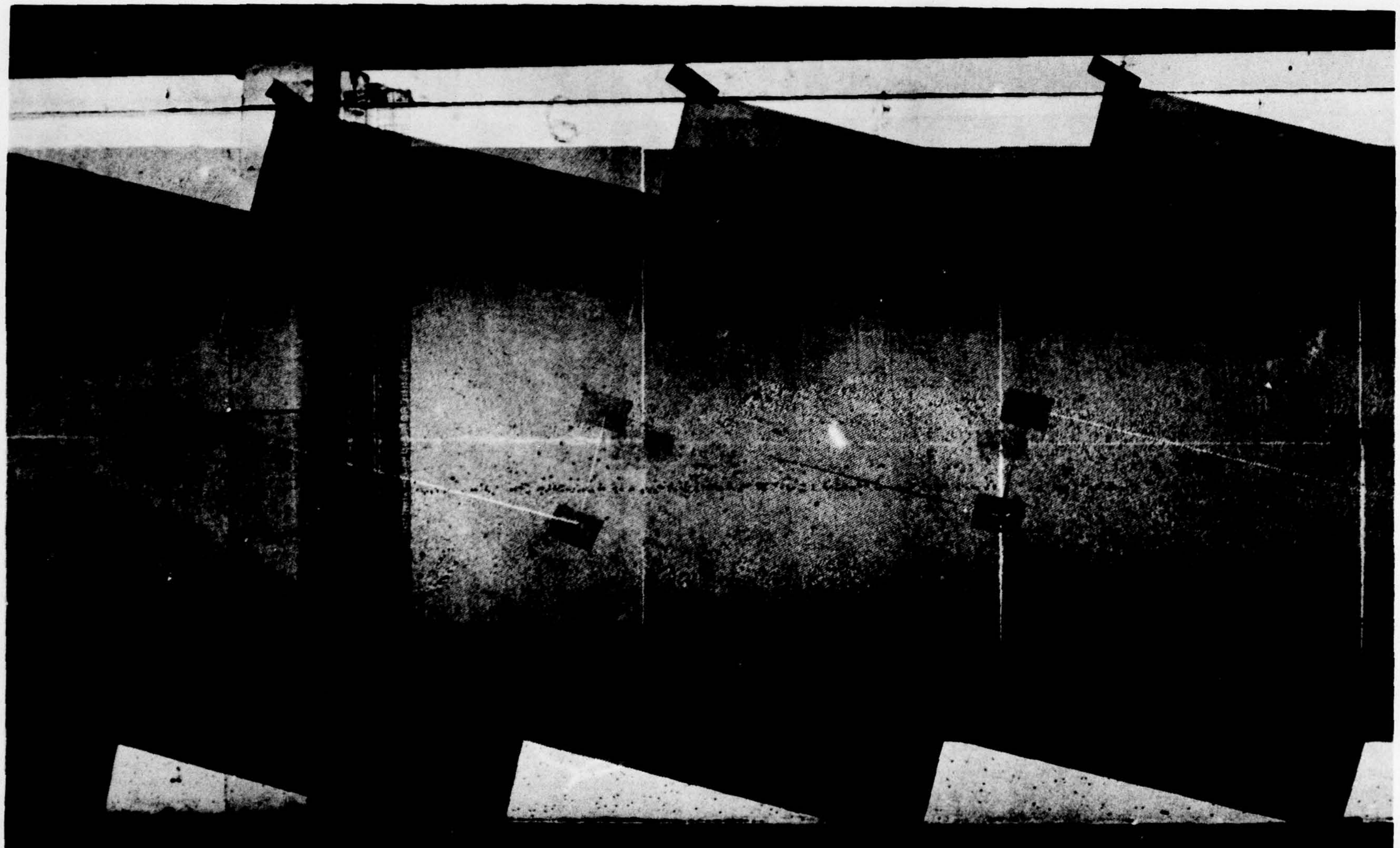

Fig. 12. Dye streaks and moire fringes in Run 6; $\frac{\Delta b_0}{g} = .01$, $t = 62.0$ sec.

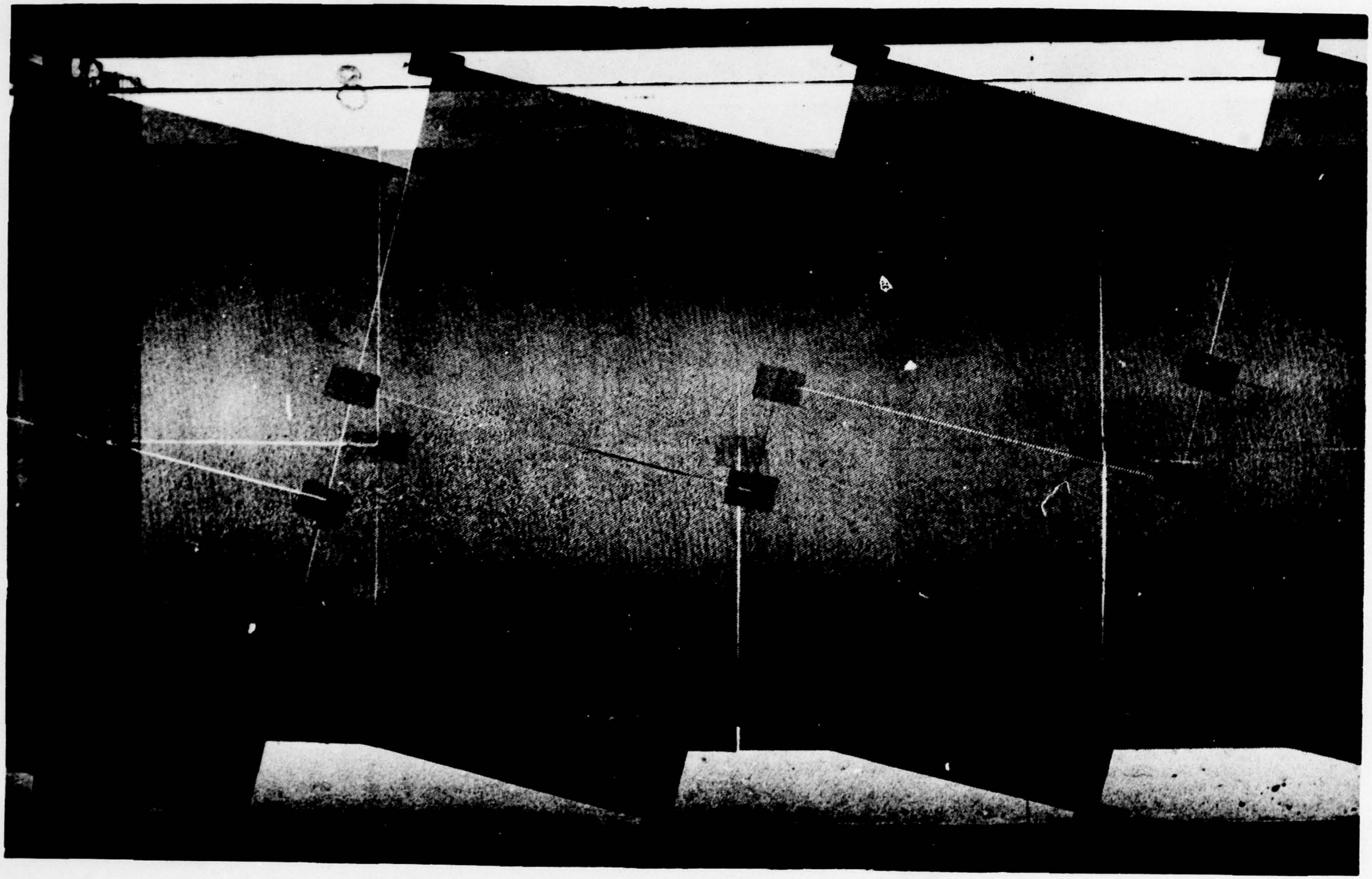

Fig. 13. Dye streaks and moire fringes in Run 8; $\frac{\Delta b_0}{g} = .0025$, $t = 253.8$ sec.

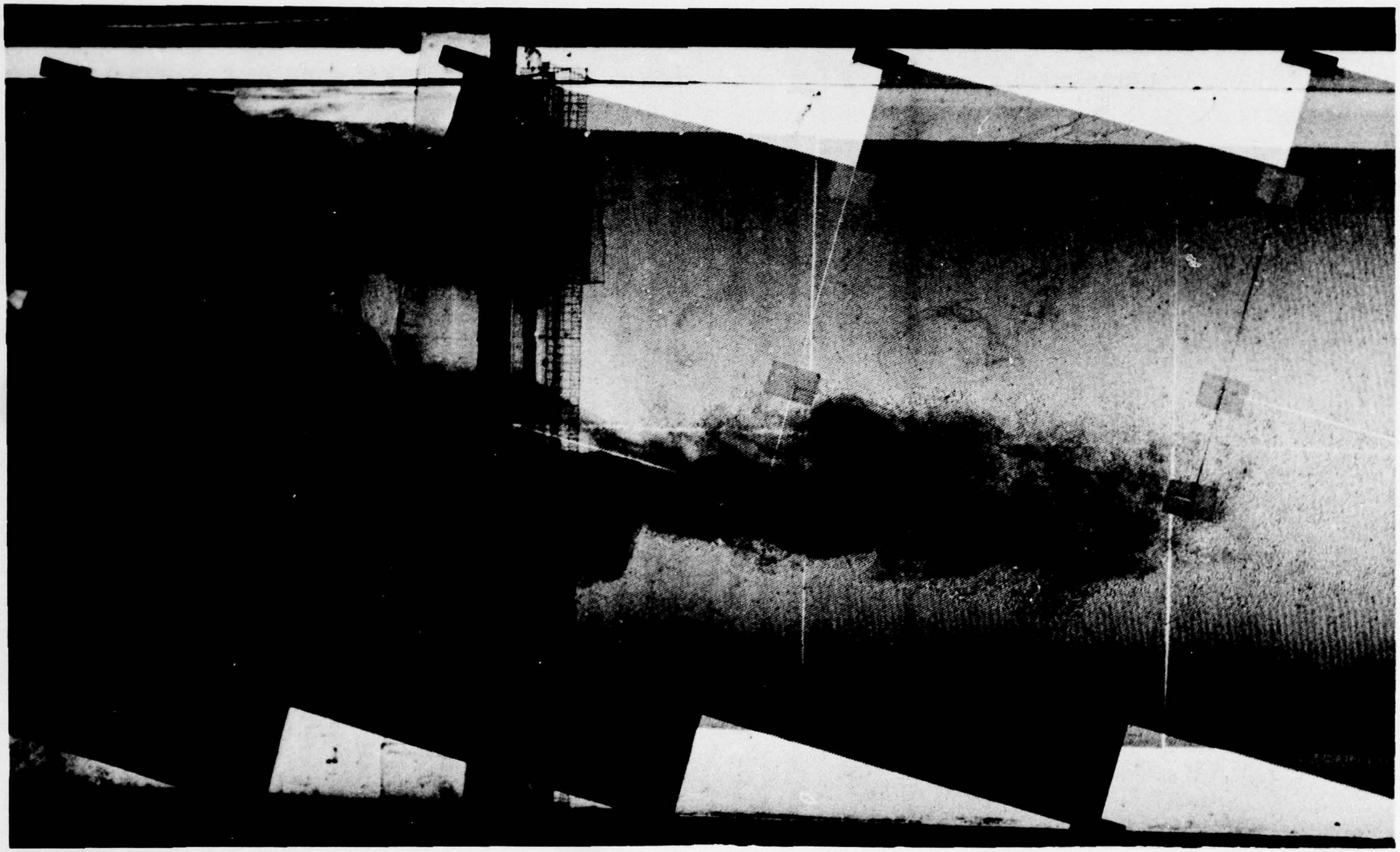

Fig. 14. Dye beginning to leave the estuary in Run 7; $\frac{\Delta b_o}{g} = .01$, $t = 131.2$ sec.

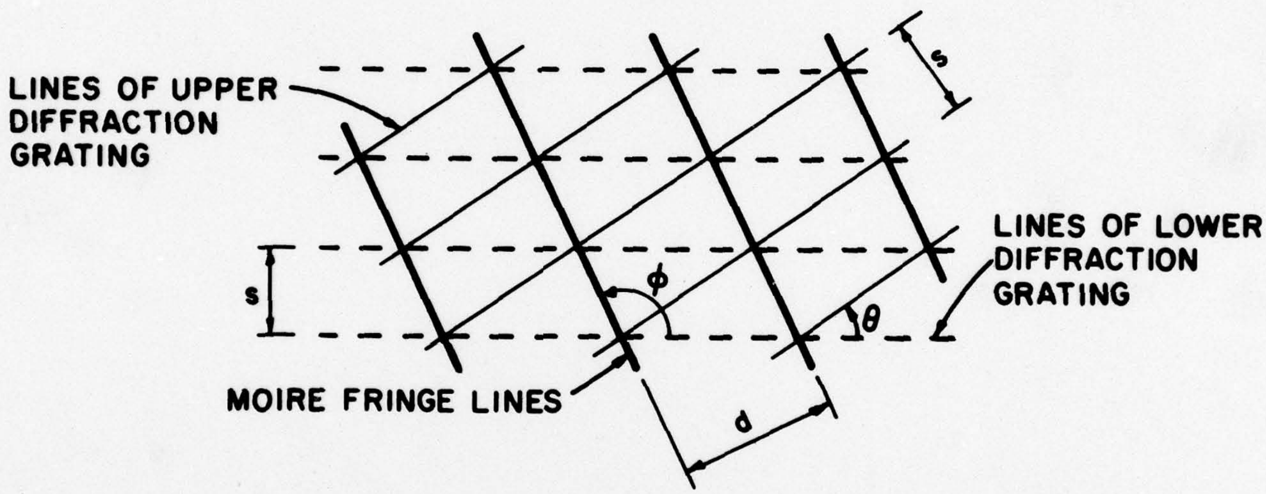

Fig. 15. Moire fringe pattern produced with two diffraction gratings.

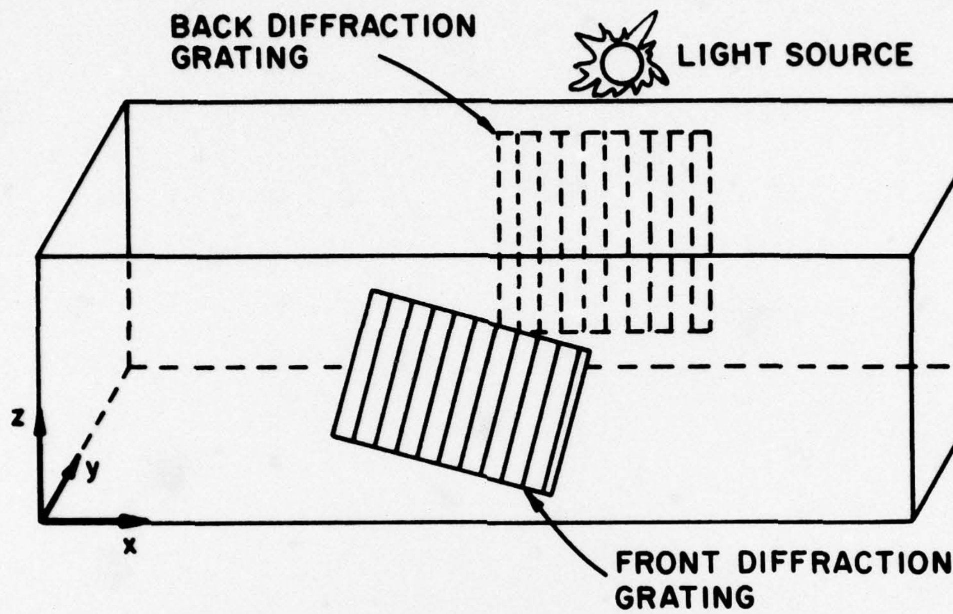

Fig. 16. A glass tank with diffraction gratings on its front and back surfaces.

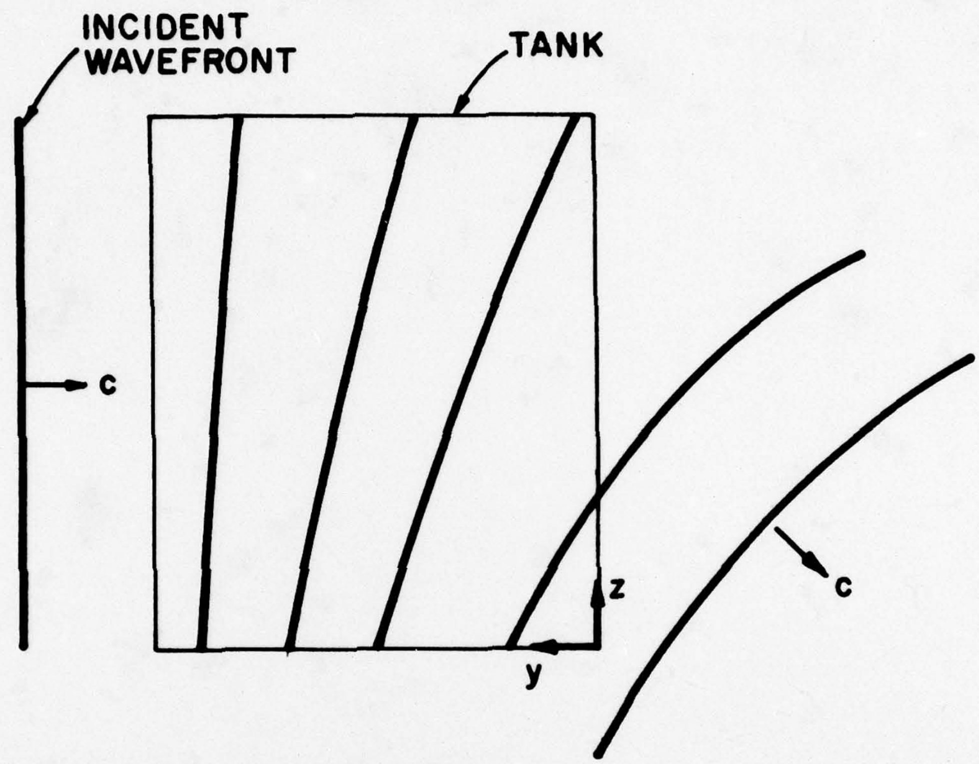

Fig. 17. Incident planar wavefronts are rotated while traversing the tank.

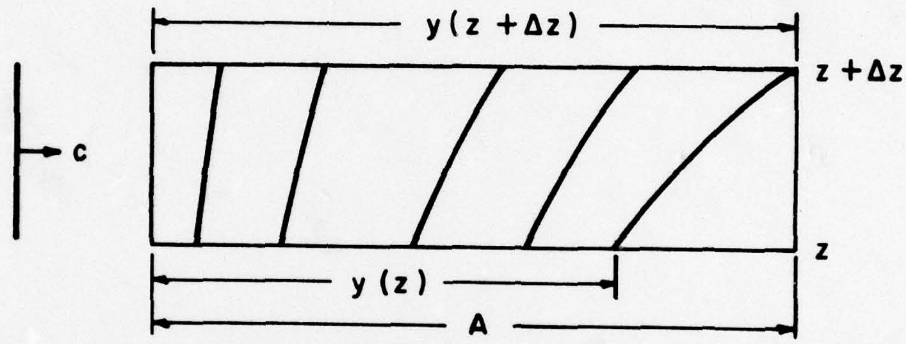

Fig. 18. Wavefront traversing segment of the tank bounded by the planes z and z+ Δz.

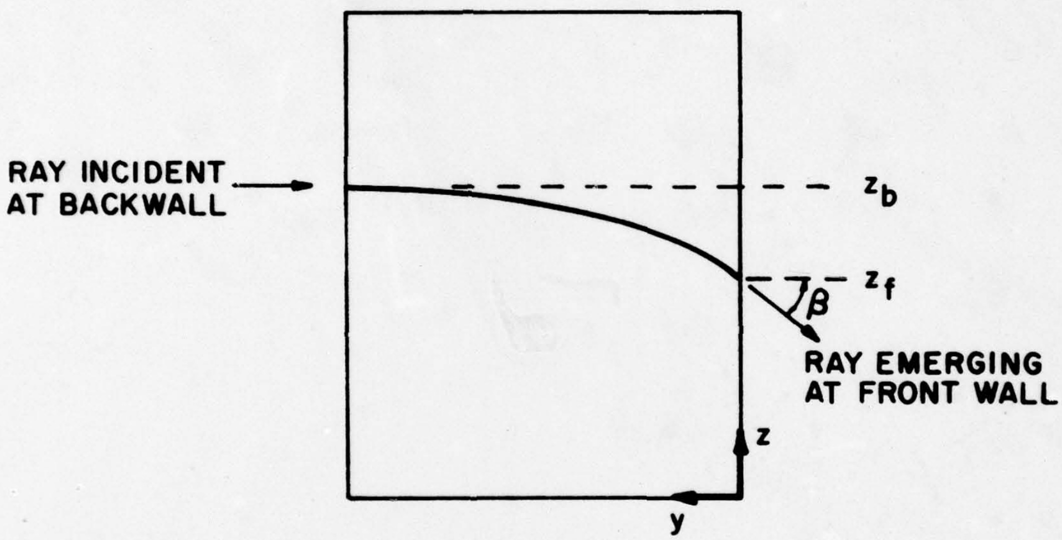

Fig. 19. A ray of light traversing the tank.

Table 1. Volumetric fluxes in cm^3/sec at $x = 22.0$ cm.

	$\Delta b_o/g$	q_o experimental	q_1 experimental	q_2 experimental	q_o, q_2 theoretical	q_1 theoretical
Run 6	.01	-84.1*	**	-101*	-90.	180
Run 7	.01	-79.0*	**	- 84.3*	-90.	180
Run 8	.0025	-38.9*	**	- 54.6*	-45.	90

*Incomplete velocity data was obtained in this layer; hence, these values are low estimates.

**No velocity data was obtained in this layer.

Table 2. Volumetric fluxes in cm^3/sec at $x = 37.0$ cm.

	$\Delta b_o/g$	q_o experimental	q_1 experimental	q_2 experimental	q_o, q_2 theoretical	q_1 theoretical
Run 6	.01	-99.3*	**	- 90.4*	-90.	180
Run 7	.01	-83.1*	**	- 97.4*	-90.	180
Run 8	.0025	-44.5	118.	-49.8	-45.	90.

Table 3. Volumetric fluxes at $x = 22.0$ cm; comparison between theory and experiment***

	$\Delta b_o/g$	Percent difference in q_o ****	Percent difference in q_1 ****	Percent difference in q_2 ****
Run 6	.01	7 *	**	-11 *
Run 7	.01	14 *	**	7 *
Run 8	.0025	16 *	**	-18 *

***A negative (positive) value indicates that the theoretical prediction is lower (higher) in absolute value than the experimental result.

****Absolute values are compared.

Table 4. Volumetric fluxes at x = 37.0 cm; comparison between theory and experiment. ***

	$\Delta b_o/g$	Percent difference in q_o ****	Percent difference in q_1 ****	Percent difference in q_2 ****
Run 6	.01	-9 *	**	0 *
Run 7	.01	8 *	**	-8 *
Run 8	.0025	1	-24	-10

Table 5. Thickness of the outgoing layer; comparison between theory and experiment.

	$\Delta b_o/g$	$1-\eta_o-\eta_1$ experimental	a experimental	$1-\eta_o-\eta_1$ theoretical	a theoretical
Run 6	.01	0.43	0.16	0.50	0.0458
Run 8	.0025	0.51	0.23	0.50	0.0458

BIBLIOGRAPHY

Baker, D. J., 1969 The use of moire fringes in laboratory oceanography. J. Marine Research, 27, 3, 361-366.

Long, R. R., 1975 Lectures on Estuarine Circulations and Mass Distributions. The Johns Hopkins University Technical Report No. 9, Series C.

__________, 1977 Three-layer circulations in estuaries and harbors. J. Phys. Oceanogr., 7, 3, 415-421.

Oster, G., Wasserman, M. and Zwerling, C., 1964 Theoretical interpretation of moire patterns. J. Optical Society of America, 54, 2, 169-175.

Stommel, H. and Farmer, H. G., 1952 Abrupt change in width in a two-layer open channel flow. J. Marine Res., 11, 205-214.

__________________________, 1953 Control of salinity in an estuary by a transition. J. Marine Res., 12, 13-20.

Van Oss, C. J., 1964 The use of gratings producing moire patterns for measuring refractive index gradients. J. Sci. Instrum., 41, 227-228.

VITA

The author was born on May 12, 1951 in Brooklyn, New York. He received a Bachelor of Engineering Degree in Engineering Science at S.U.N.Y. at Stony Brook in 1972. The author earned a Master of Science in Engineering Degree from the Department of Applied Mechanics at the University of Michigan in 1974. At the University of Michigan, he was employed as a Research Assistant and Teaching Fellow. The next two years were spent employed in the Solid Mechanics Department at the Oak Ridge National Laboratory in Oak Ridge, Tennessee. His work there primarily involved the analysis of pressure vessels for nuclear power plants. He has been a graduate student in the Department of Mechanics and Materials Science at The Johns Hopkins University from 1976 until the present. He has been employed by the University as a Research Assistant and Teaching Assistant.

Security Classification

DOCUMENT CONTROL DATA - R & D

(Security classification of title, body of abstract and indexing annotation must be entered when the overall report is classified)

1. ORIGINATING ACTIVITY (Corporate author) The Johns Hopkins University	2a. REPORT SECURITY CLASSIFICATION Unclassified
	2b. GROUP

3. REPORT TITLE

An Experimental Study of Three-Layer Circulation

4. DESCRIPTIVE NOTES (Type of report and inclusive dates)

Technical Report, July 1978

5. AUTHOR(S) (First name, middle initial, last name)

Martin N. Raftenberg

6. REPORT DATE	7a. TOTAL NO. OF PAGES	7b. NO. OF REFS
July 1978	49	7

8a. CONTRACT OR GRANT NO. N00014-75-C-0805	9a. ORIGINATOR'S REPORT NUMBER(S) Technical Report No. 14 (Series C)
b. PROJECT NO.	
c.	9b. OTHER REPORT NO(S) (Any other numbers that may be assigned this report)
d.	

10. DISTRIBUTION STATEMENT

Approved for public release. Distribution unlimited

11. SUPPLEMENTARY NOTES	12. SPONSORING MILITARY ACTIVITY Office of Naval Research

13. ABSTRACT

A "three-layer circulation" flow, which occurs typically in estuaries, was modelled in the laboratory. The experiments were designed to test theoretical predictions made by Long in an earlier analysis of the problem.

The experiment consisted briefly of the following: a tank of length 496.6 cm and cross-section 37.2 cm x 15.9 cm was filled with two layers of water, each of 15.0 cm depth. The upper layer was fresh water and the lower layer was an NaCl-water solution with .25% or 1.00% salinity. After filling was completed, a 126.3 cm length at one end of the tank was blocked off, and the two fluid layers in this region were then throgoughly mixed, resulting in a homogeneous solution having salinity .125% or .50%. The partition separating the mixed region from the rest of the tank was removed, and a three-layer circulation flow ensued. Basically, fluid from the mixed region, having a density intermediate between the two layers outside of this region, was seen to flow out along the interface of these two layers. Simultaneously, flow in the reverse direction (into the mixed region) from the external layers was observed to occur.

Several techniques were used to visualize and study the flow. Potassium permanganate pellets were dropped into the tank from above. These produced dyed material lines upon dissolving, which were then photographed and used to determine velocity profiles. The velocity profiles were integrated to obtain estimates of fluxes. Moire fringe patterns were used to visualize interfaces between regions of differing salinities as well as regions of turbulence. Finally, potassium permanganate dye in liquid form was added into the mixed region to visualize the cross-section of the outgoing slug of fluid.

Security Classification

14 KEY WORDS	LINK A		LINK B		LINK C	
	ROLE	WT	ROLE	WT	ROLE	WT
Three-layer circulation flow Estuary experiment Density current Hydraulic jump						

DD FORM 1 NOV 65 1473 (BACK)
(PAGE 2)

Security Classification